Desalination and Water Treatment
www.deswater.com

39 (2012) 21–32
February

doi: 10/5004/dwt.2012.2263

Taylor & Francis
Taylor & Francis Group

Study of falling film evaporation process in a vapor compression desalination system

Rubina Bahar[a], M.N.A. Hawlader[b,*]

[a]*Department of Mechanical Engineering, National University of Singapore, 9 Engineering Drive 1, Singapore 117576*
[b]*Department of Mechanical Engineering, International Islamic University Malaysia, Jalan Gombak, 53100 Kuala Lumpur, Malaysia*
Tel. +603 6196 6518; Fax: +603 6196 4455; e-mail: mnahawlader@gmail.com, mehawlader@iium.edu.my

Received 29 September 2010; Accepted 31 August 2011

ABSTRACT

An analysis of falling film evaporation of saltwater has been carried out for a vapor compression desalination pilot plant. Detailed modeling and simulation have been used to find the temperature and concentration variation inside the film on a vertical tube evaporator. The heat and mass transfer phenomenon were analyzed using basic conservation equations. To evaluate the performance of the rig, three operating variables were considered, which included the top brine temperature (TBT), compressor speed and brine concentration. Performance of the rig was dominated by compressor speed and top brine temperature. The highest distillate production rate experimentally obtained was 20 kg/h for the compressor speed of 2400 rpm at a TBT of 102°C. From the simulation, it was found that the feed concentration rapidly increased near the falling film-vapor interface. The numerical results have been compared with the experimental values in terms of distillate produced, and good agreement was found.

Keywords: Vapor compression desalination; Falling film evaporation; Concentration profile; Temperature profile; Vertical tube evaporator

1. Introduction

As a process of freshwater production, desalination methods are making rapid progress with the advancement in thermal and membrane technologies. Among the various desalination processes, thermal distillation methods still produce the highest amount of potable water regardless of the advancement in membrane processes. Vapor compression distillation is an efficient thermal distillation method that boosts up the thermal energy by means of compressing vapor and uses it as a heat source for evaporation. The feed water is supplied inside evaporator tubes in the form of thin falling film for better heat and mass transfer. Numerous research studies have been performed in the area of heat and mass transfer processes of the vertical falling film. Some of these researches included modeling and simulation of the evaporation process, and others focused on the performance of the system with changing parameters. The work of Raach and Mitrovic presented model development of evaporating falling film over a vertical plate heated by steam in multi effect desalination (MED) plant [1]. Nusselt's theory was utilized to obtain the velocity profile and the temperature distribution. Variation of the plate temperature along the length was a significant factor for this study. Fahem et al. and Ben Jabrallah et al. presented the numerical analysis of coupled heat and mass transfer for a rectangular saline water distillation

*Corresponding author.

cell [2,3]. The mass flux variations in the liquid film and vapor region were presented. As the film was considered very thin, the temperature variation along the film was neglected [2]. Assad and Lampinen presented a mathematical model of evaporation process from a laminar falling liquid film on a constant temperature vertical plate [4]. The vapor pressure drop, vapor exit velocity and cooling rate were calculated for different liquid mass flow values. Tsay and Lin carried out a combined numerical and experimental analysis to explore the heat and mass transfer characteristics in a laminar gas stream flowing over an evaporating falling film of water on a vertical heated plate [5]. It was found that the heat transfer between the liquid film and gas stream was dominated by the transport of latent heat with the evaporation of the liquid film. Hughes and Bott developed a model to calculate the geometry of falling fluid film for the effective use of transfer surface [6]. The expression for overall heat transfer was also found and it was dependant on tube radius, film thickness and the liquid heat transfer coefficient. Ganic and Roppo presented the result of experimental investigation of sub-cooled water films flowing down a vertical tube [7]. Heat transfer coefficient and film break down heat flux data were also found. Parametric studies to observe the performance of falling film evaporation process were carried out by Aly et al., Jin et al. and Al-Ansari and Owen [8–10]. Aly et al. studied heat transfer and fluid hydrodynamic characteristics of falling-film evaporation of natural seawater recirculation inside evaporator [8]. The production enhanced with increased steam temperature and lower concentration. Jin et al. presented the results of experimental study on the heat transfer of falling seawater film flowing over a doubly fluted plate in an MED system [9]. The effects of the temperature difference and feed water flow rate were studied with a given steam flow rate. The effect of steam flow rate was also studied under fixed feed water flow rate. Al-Ansari and Owen presented the hydrodynamic and thermal analysis for the case of a horizontal tube with the liquid outside/steam inside arrangement [10]. A three dimensional physical model was developed and solved using the equations of continuity, momentum and energy for both the internal and external processes. Several parameters including local values of heat transfer coefficient and film thicknesses were calculated.

Although there have been many studies on the heat transfer process of falling film evaporation, the change in concentration of the feed did not draw significant attention for a desalination process. In this study, the falling film evaporation process of saline water inside vertical tubes has been analyzed and the results were validated for a 2 stage vapor compression MED pilot plant. The changes in temperature and concentration along and across the falling film inside the evaporator have been completely analyzed. The results from the simulation have been validated on the existing vapor compression desalination unit in terms of produced distillate.

2. Experiments

The desalination setup consists of two identical evaporator- condenser assemblies termed as Effects. Fig. 1 shows the schematic diagram of the existing setup. The compressor outlet is connected to Effect 1 and the suction side is connected to Effect 2, where effect 1 operated at a higher temperature and pressure than that of Effect 2.

Inside the evaporator, there are 6 vertical tubes. From feed tank, the brine is delivered to the bottom chamber of the Effects. From there, it is delivered to the top of each Effect through the recirculation pump. On the way, the electric heaters heat up the solution to the preset temperatures.

The hot solution passes through some flow restrictors to form a falling brine film. The setup is run and vented continuously until there is enough steam generated inside Effect 2 to reach the compressor. Once there is sufficient steam in the line, the vapor compressor starts drawing vapor from evaporator side of Effect 2 and delivers to the condenser side of Effect 1.

Inside Effect 1, the falling film of brine travels along the tube wall and absorbs additional heat from the tube wall where the condensing vapor gives away its latent heat to form the distillate. The brine solution absorbs the latent heat of condensation and gets evaporated to generate more steam. The rest of the brine falls down to the bottom of the Effect where it gets mixed with the incoming feed and then re-circulated again to the top of the Effect.

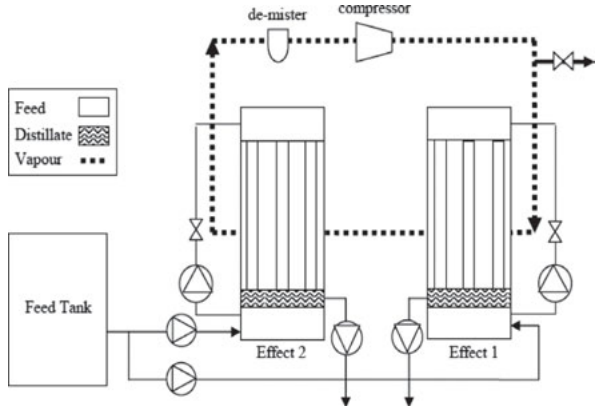

Fig. 1. Schematic of the Setup.

The vapor generated from Effect 1 goes to Effect 2 and condenses on the outer shell of the tubes. Since operating pressure inside Effect 2 is lower than that in Effect 1, the vapor from Effect 1 travels to Effect 2 through natural draft. The cycle repeats again inside Effect 2 but at a lower pressure and temperature. The vapor generated from Effect 2 goes to the compressor suction through the de-mister and the distillate is collected from Effect 2 condenser.

The six evaporator tubes form a circle shown in Fig. 2. The re-circulated brine first falls on a perforated plate that is placed on top of the evaporator tubes. Below the plate, there is a tubular groove attached on top of each evaporator tubes, as shown in Fig. 2. The grooves are positioned in such a way that the outer wall of the groove is in close contact with inner wall of the tubes with a small allowance.

The groove design is vital to establish a proper falling film. These grooves are closed at the ends but have holes around their walls. The solution is not allowed to pass directly through the groove because of the closed end and rather forced to escape through the holes around the groove wall. Thus small amount of brine is allowed to pass through the annular space between the tube and the groove, and a thin falling film of brine is established inside the tube. The operating variables include top brine temperature (TBT), vapor compressor speed and brine concentration. The TBT was varied from 99°C to 103°C for Effect 1 and 97°C to 101°C for Effect 2. The compressor speed was varied between 1500 rpm and 2400 rpm and the brine concentration was varied from 20,000 ppm to 33,000 ppm. Brine recirculation rate was kept constant at 0.205 kg/s.

2.1. Experimental uncertainties

The instruments used in the experiments had the following uncertainties

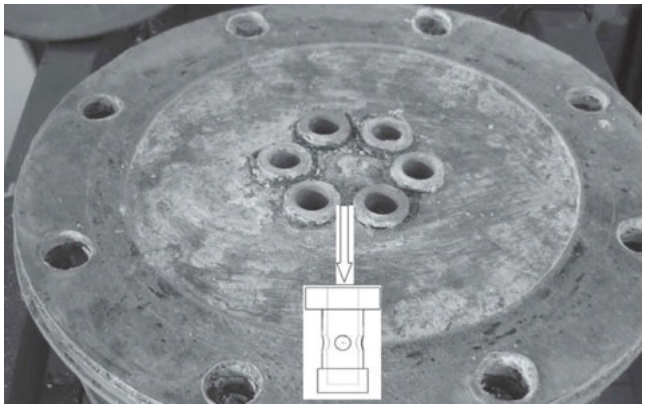

Fig. 2. Photograph of the tubular grooves on the evaporator tubes.

Thermocouple: $\pm$ 0.5°C.

Pressure gage: $\pm$1% of gauge reading.

The instrument error $\delta T_1 = \pm 0.5$°C is the uncertainty associated with the thermocouples, while the random error δT_2 is given by $\delta T_2 = \sum_1^n \frac{\left(T_s - \overline{T}\right)}{n-1}$ where n is the number of data taken to determine T_s, $\overline{T}$ is the mean of the population.

3. Modeling of the falling film evaporation process

This section presents a description of the mathematical model of the evaporation phenomena inside the tubes. Fig. 3 shows the geometry and the process of evaporation. The saline water enters the evaporator with a salt mass fraction of C_{NaCl}. While the solution travels along the heated evaporator wall, it gets evaporated and the vapor mass flux travels away from interface due to the difference in partial vapor pressure. This evaporation process continues along the length of the tube and the solution at the outlet becomes concentrated. The tube wall was considered to be at constant temperature as a result of condensation taking place on the outer wall. The entire process was considered to be in steady state, laminar region. In the figure, it is shown that the flow was over a vertical flat plate. The value of calculated film thickness was very small.

The heat transfer rate from the cylindrical surface compared to that from a flat plate for this thin film varied by only 2.5%. Hence, curvature effect of the tube for heat

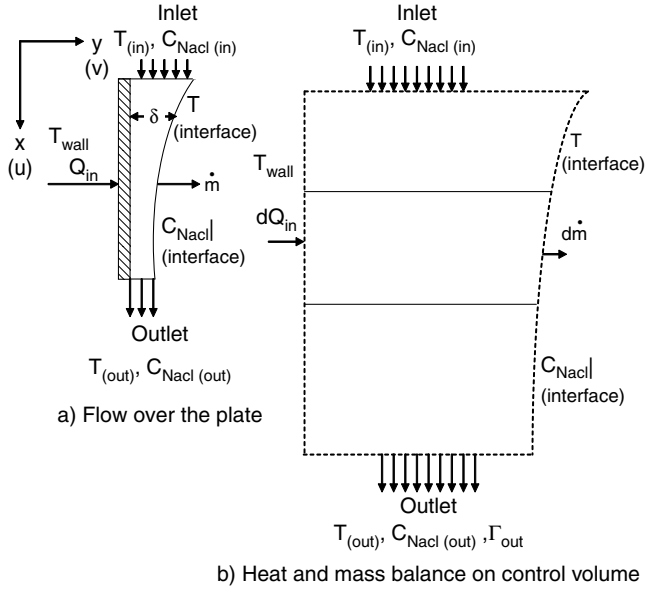

Fig. 3. The falling film evaporation process.

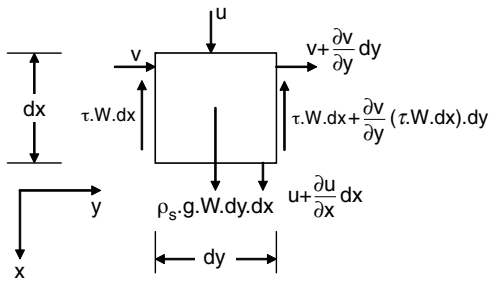

Fig. 4. Force balance on the small element inside film.

transfer was neglected to avoid unnecessary complexities in the computational work. Also, it was assumed no presence of wave formation or film breakage.

The conservation equations of mass, momentum and energy have been employed to derive the different equations. An elemental control volume is considered inside the falling film and the forces acting on it are shown in Fig. 4. The solution flows along x axis and the film is developed along the y axis. The depth of the control volume is W. Two velocities u and v, have been considered along x and y directions, respectively.

The continuity Equation

For steady-state condition, a mass balance on the control volume gives:

$$\frac{\partial u}{\partial x} + \frac{\partial v}{\partial y} = 0 \tag{1}$$

The momentum equation

From the conservation of momentum,

Σforces = rate of change of momentum

The final form of momentum equation for a falling film process becomes

$$-\frac{\partial \tau}{\partial y} + \rho_s g = 0 \tag{2}$$

The energy equation

An energy balance over the control volume neglecting heat conduction in the direction of flow and the viscous work gives the energy equation:

$$\frac{\partial}{\partial x}(uT) + \frac{\partial}{\partial y}(vT) = \alpha \frac{\partial^2 T}{\partial y^2} \tag{3}$$

The mass transfer equation

Similar to the energy equation, the mass transfer equation is written as

$$\frac{\partial}{\partial x}(uC_{\mathrm{NaCl}}) + \frac{\partial}{\partial y}(vC_{\mathrm{NaCl}}) = D_s \frac{\partial^2 C_{\mathrm{NaCl}}}{\partial y^2} \tag{4}$$

where D_s is the diffusion coefficient of NaCl in the solution.

The boundary conditions required to solve the governing equations are:

1. At $x = 0$, i.e., at the entrance,

$$C_{\mathrm{NaCl}} = C_{\mathrm{NaCl}}\,|_{\mathrm{entrance}};\ T = T_{\mathrm{o}},\text{and } \Gamma = \Gamma_{\mathrm{o}}, \tag{5}$$

2. At $y = 0$, i.e., at the wall

$$u = 0; v = 0; \frac{\partial C_{\mathrm{NaCl}}}{\partial y} = 0 \text{ and } T = T_{\mathrm{wall}}, \tag{6}$$

3. At $y = \delta$, i.e., at the interface:

$$\frac{\partial u}{\partial y} = 0; \tau = 0 \tag{7}$$

4. The boundary condition for evaporation at the interface is found applying the method described by Islam as [11]:

$$v_{\mathrm{water}}\rho_{\mathrm{water}} = v_{\mathrm{solution}}\rho_{\mathrm{water}} + \rho_s D_s \frac{\partial C_{\mathrm{water}}}{\partial y}\Big|_{y=\delta}$$

$$v_{\mathrm{water}}\rho_{\mathrm{water}} = \rho_{\mathrm{water}} \frac{v_{\mathrm{water}}.\rho_{\mathrm{water}} + v_{\mathrm{NaCl}}.\rho_{\mathrm{NaCl}}}{\rho_s} + \rho_s D_s \frac{\partial C_{\mathrm{water}}}{\partial y}\Big|_{y=\delta} \tag{8}$$

since $v_{\mathrm{NaCl}} = 0$, Eq. (8) becomes

$$\dot{m} = \frac{\rho_{\mathrm{water}}}{\rho_s}\dot{m} + \rho_s D_s \frac{\partial C_{\mathrm{water}}}{\partial y}\Big|_{y=\delta}$$

$$\dot{m} = C_{\mathrm{water}}\dot{m} + \rho_s D_s \frac{\partial C_{\mathrm{water}}}{\partial y}\Big|_{y=\delta} \tag{9}$$

$$\dot{m} = \frac{\rho_s D_s}{1 - C_{\mathrm{water}}} \frac{\partial C_{\mathrm{water}}}{\partial y}\Big|_{y=\delta}$$

Using $C_{\mathrm{NaCl}} + C_{\mathrm{water}} = 1$, Eq. (9) becomes

$$\dot{m} = -\frac{\rho_s D_s}{\delta\, C_{\mathrm{NaCl}}} \frac{\partial C_{\mathrm{NaCl}}}{\partial y}\Big|_{y=\delta} \tag{10}$$

For interface temperature, an additional boundary condition has been found from the work of Grossman which shows interface temperature has a linear relationship with interface concentration [12]:

$$T\Big|_{y=\delta} = aC_{\mathrm{NaCl}}\Big|_{y=\delta} + b \tag{11}$$

The values of a and b corresponding to variable evaporator pressure are tabulated in Table 1 as

For heat transfer at the interface,

$$\dot{q}\Big|_{y=\delta} = \dot{m}\, h_{fg} = k_s \frac{\partial T}{\partial y}\Big|_{y=\delta} \tag{12}$$

3.1. Derived expressions for different parameters

Before moving into the solution of energy and mass transfer equations numerically, the expressions for different parameters like the velocities in the two directions, film thickness and heat transfer coefficients were required.

3.1.1. Velocities

The two velocities u and v have been derived solving the momentum and continuity equations respectively.

For velocity u, Eq. (2) has been used by Bird et al. which yields [13]:

$$\frac{\partial u}{\partial y} = \frac{\rho_s g}{\mu}(\delta - y) \tag{13}$$

Integrating Eq. (13) with the boundary conditions stated in Eq. (7) gives

$$u = \frac{g}{\upsilon}\left(\delta y - {}^{y^2}\!/_{2}\right) \tag{14}$$

where $\upsilon = \mu/\rho s$ the kinematic viscosity.

To find the velocity v, mass continuity Eq. (1) has been utilized by Islam and the expression for v is found as [11]

$$v = -\frac{g}{2\upsilon}\frac{\partial \delta}{\partial x} y^2 \tag{15}$$

3.1.2. Film thickness

To find an expression for film thickness, the average value of velocity u has been used by Bird et al. [13].

Table 1
Coefficients for equilibrium temperature-salt concentration relation (at different evaporator pressures)

Pressure (bar)	0.8	0.85	0.90	0.95	1.0	1.05
a	17.74	19.002	19.847	21.114	19.988	17.526
b	94.07	95.118	96.743	98.356	99.901	100.47

$$u_{\mathrm{ave}} = \frac{\int_0^{\delta} u\partial y}{\int_0^{\delta} \partial y}$$

After integration, the term becomes

$$u_{\mathrm{ave}} = \frac{g\delta^2}{3\upsilon} \tag{16}$$

The volume flow rate inside the tube,

$$Q = W\,\delta\, u_{\mathrm{ave}} \tag{17}$$

Combining Eq. (16) and (17) gives

$$\delta = \sqrt[3]{\frac{3.\Gamma.\upsilon}{\rho g}} \tag{18}$$

3.1.3. Heat transfer coefficients

The overall heat transfer coefficient in the evaporator side from condensing vapor is a combination of convective heat transfer coefficients and resistance offered by wall thickness. According to Islam, two types of convective heat transfer coefficients are present during the process [11]. One is between the wall and the bulk fluid, the other is between the bulk fluid and solution at interface.

The convective heat transfer coefficient between wall and bulk fluid, h_w is expressed by

$$h_w(T_{\mathrm{wall}} - T_{\mathrm{bulk}}) = k_s \frac{\partial T}{\partial y}\Big|_{y=0} \tag{19}$$

The convective heat transfer coefficient between the bulk fluid and interface is given by h_i which is expressed as

$$h_i(T_{\mathrm{bulk}} - T_{\mathrm{interface}}) = k_s \frac{\partial T}{\partial y}\Big|_{y=\delta} \tag{20}$$

If the wall resistance is t/k_{wall} then the overall heat transfer coefficient, U becomes:

$$U = \frac{1}{\frac{1}{h_w} + \frac{t}{k_{\mathrm{wall}}} + \frac{1}{h_i}} \tag{21}$$

In order to solve these equations, the computational domain was made dimensionless and rectangular. The film thickness varied along the tube length, i.e., as the

solution traveled along the tube length, the film thickness decreased because of evaporation. Hence, to make the axis dimensionless, y values have been replaced by ψ such that $\psi = y/\delta$ and for the x axis, the x values have been substituted by the value ξ where $\xi = x/L$. Transformations have been done for the energy and mass transfer equations and the other parameters and similar transformations have been done for the boundary conditions as well.

The continuity and momentum equations have been solved earlier to obtain expressions for velocities and film thickness. The expressions in the $\xi - \psi$ coordinate become:

Film thickness,

$$\delta = \sqrt[3]{\frac{3.\Gamma\upsilon}{\rho g}} \tag{22}$$

The velocity along ξ direction,

$$u = \frac{g}{\upsilon}\left(\delta\psi - \delta^2\psi^2/2\right) \tag{23}$$

Velocity along ψ direction,

$$v = -\frac{g}{2\upsilon}\frac{\partial\delta}{\partial x}\delta^2\psi^2 \tag{24}$$

Now, $\dfrac{\partial\delta}{\partial x} = \dfrac{\partial}{\partial x}\sqrt[3]{\dfrac{3\Gamma\upsilon}{\rho g}}$

$$\frac{\partial\delta}{\partial x} = \sqrt[3]{\frac{\upsilon}{9\rho g\Gamma^2}}\cdot\frac{\partial\Gamma}{\partial x}$$

Here, $\dfrac{\partial\Gamma}{\partial x} = \dot{m}$

Hence, Eq. (24) becomes

$$v = -\frac{g\delta^2\psi^2}{2\upsilon}\dot{m}\sqrt[3]{\frac{\upsilon}{9\rho g\Gamma^2}} \tag{25}$$

The original energy equation is obtained from Eq. (3) as

$$\frac{\partial}{\partial x}(uT) + \frac{\partial}{\partial y}(vT) = \pm\frac{\partial^2 T}{\partial y^2}$$

The velocity u changes with both along the film and along the tube length, and it requires to be divided in two components for the term: $\dfrac{\partial}{\partial x}(uT)$:

$$\frac{\partial}{\partial x}(uT) = \frac{1}{L}\frac{\partial(uT)}{\partial\xi} - \frac{\partial\delta}{\partial x}\frac{\psi}{\delta}\frac{\partial(uT)}{\partial\psi}$$

The operator $\dfrac{\partial}{\partial x}$ is expressed in the following form for this purpose:

$$\frac{\partial}{\partial x} = -\frac{\partial\delta}{\partial x}\frac{\psi}{\delta}\frac{\partial}{\partial\psi}$$

Hence, in the transformed coordinate after rearranging, energy equation takes the form of

$$\frac{1}{L}\frac{\partial(uT)}{\partial\xi} - \frac{\dot{m}.}{\delta}\left(\frac{\nu}{9\rho g\Gamma^2}\right)^{1/3}\left[\frac{\partial(\psi uT)}{\partial\psi} - uT\right] + \frac{\partial(\upsilon T)}{\delta.\partial\psi} = \frac{\alpha}{\delta^2}\frac{\partial^2 T}{\partial\psi^2} \tag{26}$$

In similar way, the expression for mass transfer equation may be written as

$$\frac{1}{L}\frac{\partial(uC_{\mathrm{NaCl}})}{\partial\xi} - \frac{\dot{m}}{\delta}\left(\frac{\nu}{9\rho g\Gamma^2}\right)^{1/3}\left[\frac{\partial(\psi uC_{\mathrm{NaCl}})}{\partial\psi} - uC_{\mathrm{NaCl}}\right] + \frac{\partial(vC_{\mathrm{NaCl}})}{\delta\,\partial\psi} = \frac{D_s}{\delta^2}\frac{\partial^2 C_{\mathrm{NaCl}}}{\partial\psi^2} \tag{27}$$

Boundary conditions in the transformed coordinates became:

1. At $\xi = 0$, i.e., at the entrance,

$$C_{\mathrm{NaCl}} = C_{\mathrm{NaCl}}\,|_{\mathrm{entrance},}; T = T_{\mathrm{o}}; \Gamma = \Gamma_{\mathrm{o}}, \tag{28}$$

2. At $\psi = 0$, i.e., at the wall

$$\frac{\partial C_{\mathrm{NaCl}}}{\delta\partial\dot{\mathrm{E}}} = 0 \text{ and } T = T_{\mathrm{wall}}, \tag{29}$$

3. At $\psi = 1$, i.e., at the interface:

$$\dot{m} = -\frac{\rho_s D_s}{\delta C_{\mathrm{NaCl}}}\frac{\partial C_{\mathrm{NaCl}}}{\partial\psi}\Big|_{\psi=1} \tag{30}$$

$$T_{|\psi=1} = a\,C_{\mathrm{NaCl}}\Big|_{\psi=1} + b \tag{31}$$

$$\dot{q}\Big|_{\psi=1} = \dot{m}\,h_{fg} = k_s\frac{\partial T}{\delta\,\partial\psi}\Big|_{\psi=1} \tag{32}$$

3.2. Solution method

A numerical method was employed to solve the energy and mass transfer equations and evaluate the evaporation rate, velocities, film thickness, heat transfer

coefficients and most of all, the temperature and concentration distribution along and across the film. After the axis transformation, the expressions have been discretized to apply finite-difference technique as the most convenient approach to the existing problem. MATLAB was used to solve the equations. The known inputs including feed flow rate, solution temperature, wall temperature, tube length and solution properties like viscosity, density, diffusion coefficient, conductivity were fed into the program. The calculation started with an initial guessed value of mass flux. The discretized mass transfer equation was solved first using this value. After the concentration profile was found, the discretized energy equation was solved with the known value of interface concentration, hence the interface temperature. The mass flux was re-calculated and if the guessed mass flux matched the calculated value then the calculations for next row were carried out. Otherwise, the program again started with a new guessed value of mass flux and iteration continued. Fig. 5 shows the flowchart of the program.

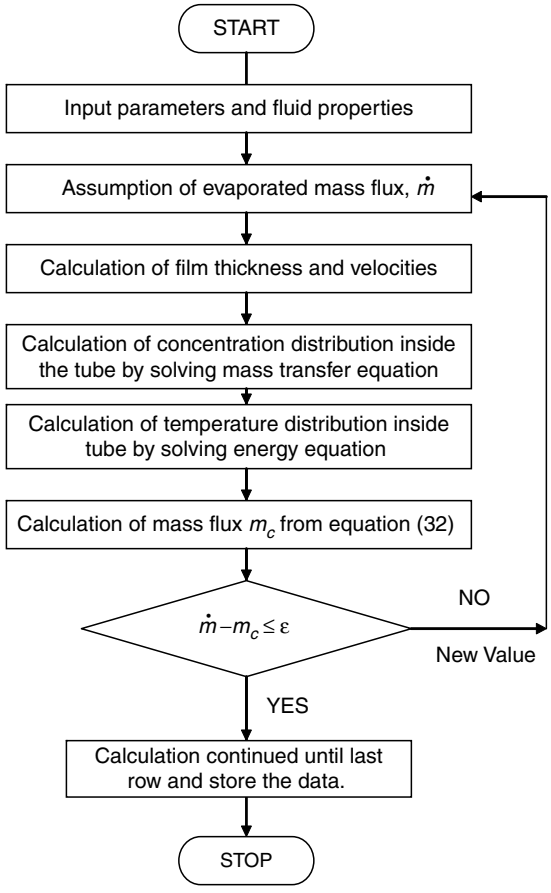

Fig. 5. Flowchart of the program.

4. Results and discussion

The simulation was utilized mainly to observe the concentration and temperature profiles, variation of film thickness, evaporation rate and heat transfer coefficients under different operating conditions. Also, validation of the model under different operating experimental conditions was accomplished.

4.1. Simulation results for concentration and temperature profiles and other parameters

4.1.1. Concentration profile

Fig. 6 shows the concentration profile obtained from the simulation. It is seen from the figure that the solution experienced a rapid concentration change near the vapor-film interface. Along the tube length, the concentration increased as a result of evaporation as the solution traveled from inlet toward outlet. A parametric study revealed that the diffusion coefficients and the inlet solution flow rate mainly influenced the concentration distribution in the film. As the diffusion coefficient of water had a very small value, the evaporation took place in the interface region and a rapid change in salt concentration was observed near the interface region only.

Also, decreasing the solution flow rate at the entrance influenced the concentration profile. The region of changing salt concentration was spread over the film thickness with lowering solution flow rate, as shown in Fig. 7. The solution velocity along the tube decreased with decreasing solution flow rate which resulted in more residence time of the falling film inside the heated tube. Since the film became thinner, heat transfer from the wall to the interface was easier due to the lower value of the film resistance. As a result, higher rate of evaporation was

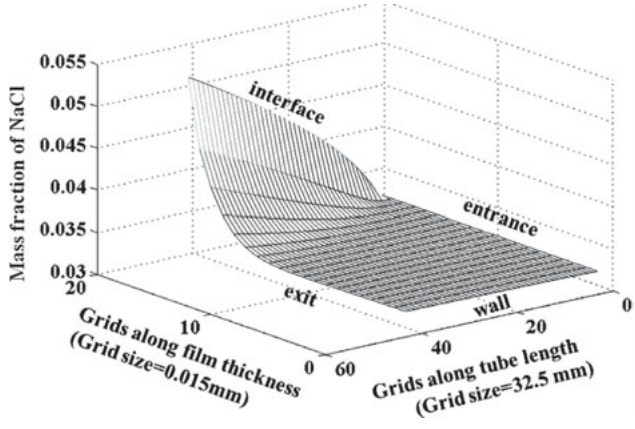

Fig. 6. Concentration profile inside evaporator tube (flow rate 2.57 kg/s m, solution temperature 102°C, tube length 1.3 m).

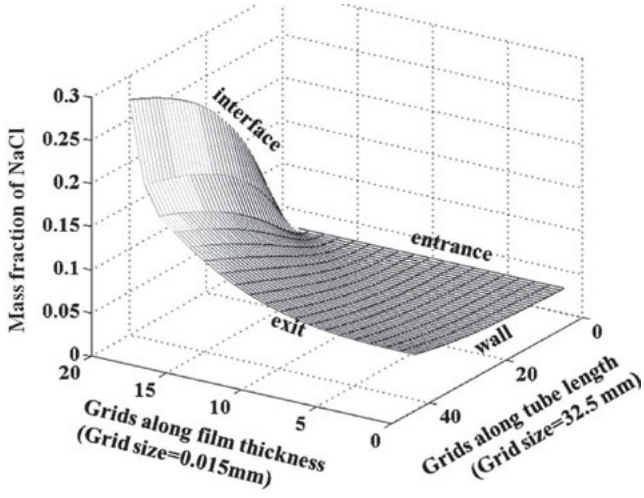

Fig. 7. Concentration profile inside evaporator tube with lower flow rate. (flow rate 0.257 kg/s m, solution temperature 102°C, tube length 1.3 m)

obtained and the change in concentration took place along the total film thickness. It is seen that the solution experienced change in concentration through the entire thickness of the film.

4.1.2. Temperature profile

Fig. 8 shows the temperature profile. The wall temperature was considered constant since steam condensed on the wall and gave its latent heat to the evaporating brine solution. The entrance temperature of the solution was 102°C. From the wall to the interface, the temperature dropped as a result of evaporation and it showed a linear pattern.

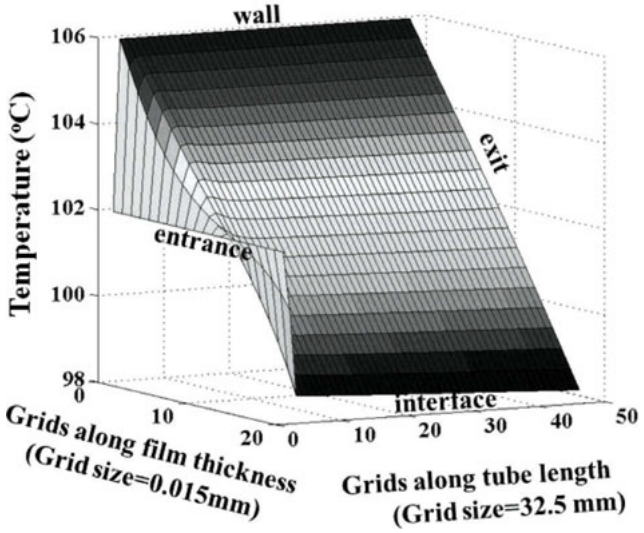

Fig. 8. Temperature distribution inside evaporator tube. (Solution inlet temperature 102°C, evaporator wall temperature 106°C, tube length 1.3 m)

4.1.3. Film thickness

The film thickness decreased linearly along the tube length, as seen in Fig. 9. The linear pattern of film thickness may be the result of two possibilities. First one may be, the tube was not long enough to complete the evaporation process. The second one may be the solution flow rate is quite high compared to the rate of evaporation. As a result, the effect of evaporation and thus the change in film thickness is not so prominent. Parametric study with changing tube length and solution flow rate was undertaken to find the possible explanation. The given input for tube length was increased up to 10 times higher than the original tube length; still the effect on film thickness was insignificant. Hence, tube length was not the factor influencing film thickness pattern. For reducing the solution flow rate, it was found that the film thickness moved toward a curved pattern which is usual for a evaporating falling film. Fig. 10 shows the film distribution along the tube with changing solution flow rate.

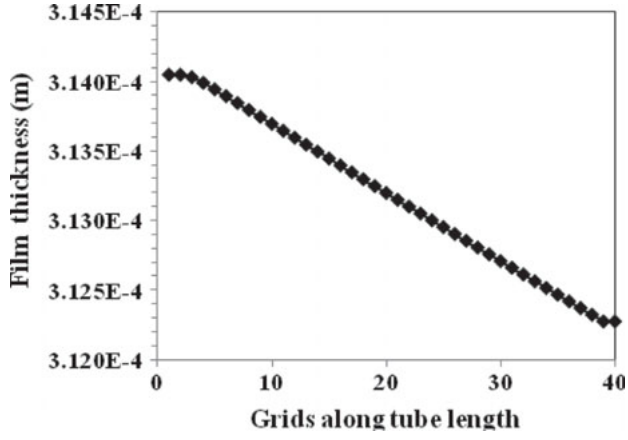

Fig. 9. Film thickness along tube length. (Solution inlet temperature 102°C, tube length 1.3 m)

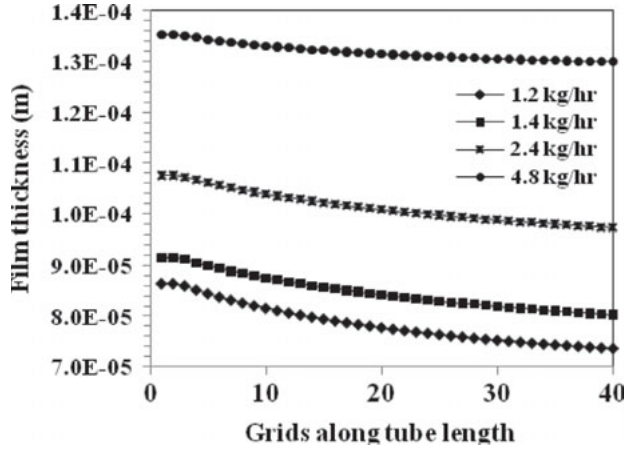

Fig. 10. Film thickness along tube length for different solution flow rate. (Solution inlet temperature 102°C, tube length 1.3 m)

4.1.4. Evaporation rate

The evaporated mass flux found from simulation is presented in Fig. 11. The rate was highest near the entrance region and then declined gradually toward the end of the tube. The reason is, near tube entrance, evaporation started after the solution absorbed heat from the wall. Hence, the solution concentration increased and corresponding boiling point also increased as a result of boiling point elevation. Along the flow path, the evaporation continued and more concentrated solution was traveling toward the end of the tube. To maintain the same evaporation rate, more heat input was required. But as the heat of evaporation was supplied from constant temperature condensation outside the tubes, it was not sufficient to overcome the higher energy requirement caused by elevated boiling point. Hence, the rate of evaporation decreased along the tube length.

Parametric study with changing solution flow rate and wall temperature was carried out to observe evaporation rate under variable operating conditions. Fig. 12 shows the effect of increasing brine recirculation on evaporation rate. It was found from the simulation that evaporation rate dropped with increasing brine recirculation. It is a consequence of increased solution velocity and the thicker film caused by increased mass flow rate. The increased velocity reduced residence time of the falling film inside the tube and increased film thickness offered higher resistance to heat transfer between wall and the film interface. Fig. 13 shows the effect of wall temperature on the evaporation rate. As expected, increasing wall temperature facilitated the evaporation rate because the heat supplied for evaporation increased with increasing wall temperature.

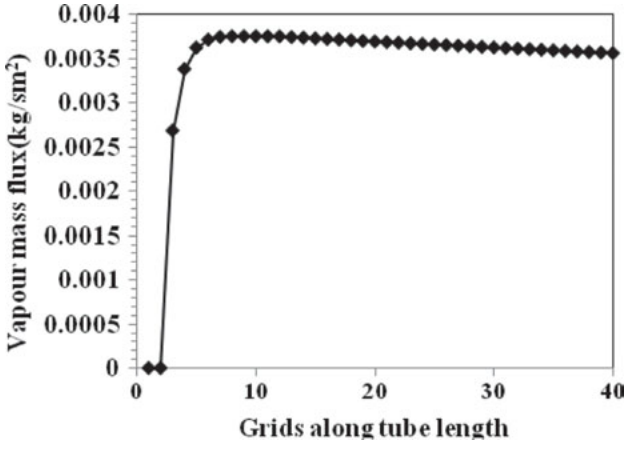

Fig. 11. Evaporation rate along tube length. (Feed inlet temperature 102°C, tube length 1.3 m)

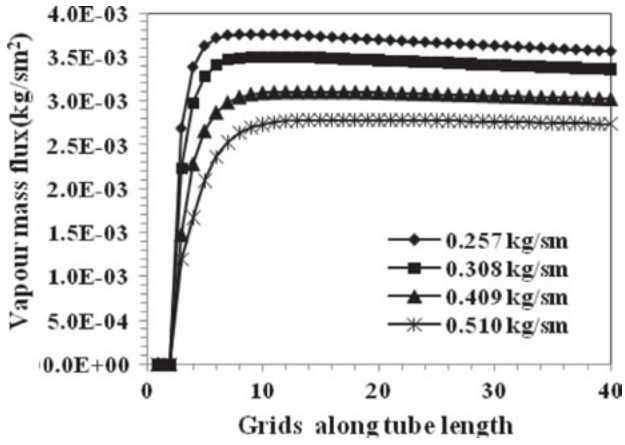

Fig. 12. Evaporation rate along tube length for different solution flow rate. (Feed inlet temperature 102°C, wall temperature 106.5°C, tube length 1.3 m)

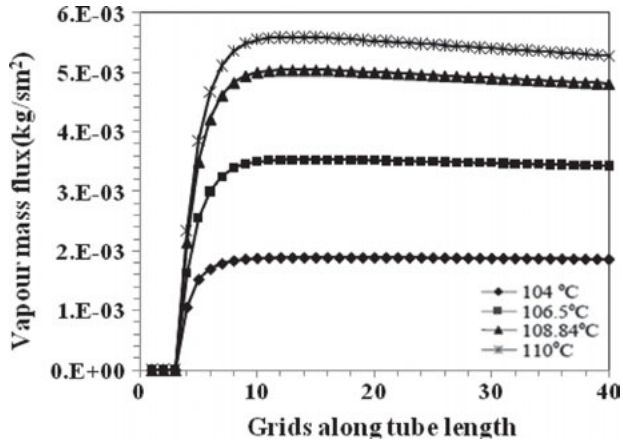

Fig. 13. Evaporation rate along tube length for different wall temperatures. (Solution inlet temperature 102°C, tube length 1.3 m)

4.1.5. Heat transfer coefficients (HTC)

The overall heat transfer coefficients with increased wall temperatures and flow rates found from simulation are presented in Figs. 14 and 15 respectively.

The overall heat transfer coefficient is a function of temperature and wall thickness. It is seen from both the figures that except for the entrance region, there is no significant variation in overall HTC values along tube the length. Fig. 14 shows the HTC values with changing wall temperature where a minor variation at the flow inlet region is observed, but within the fully developed flow region, the magnitude did not change for different wall temperatures.

Some variation in the HTC values between the different flow rates is seen in Fig. 15 with the higher solution flow rate to have lower values of HTC. With increased

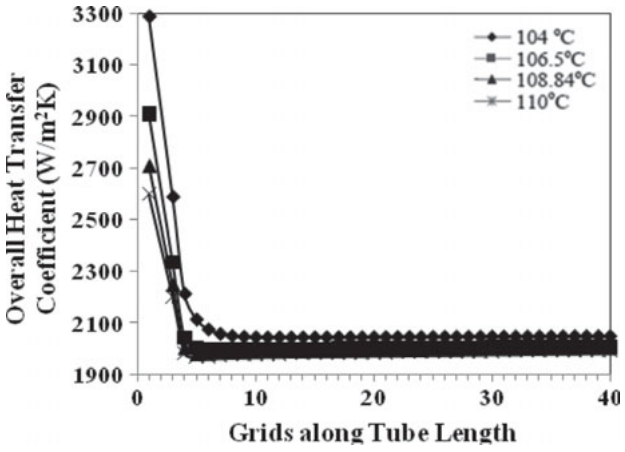

Fig. 14. Overall Heat transfer coefficient along tube length for different wall temperatures. (Solution inlet temperature 102°C, tube length 1.3 m)

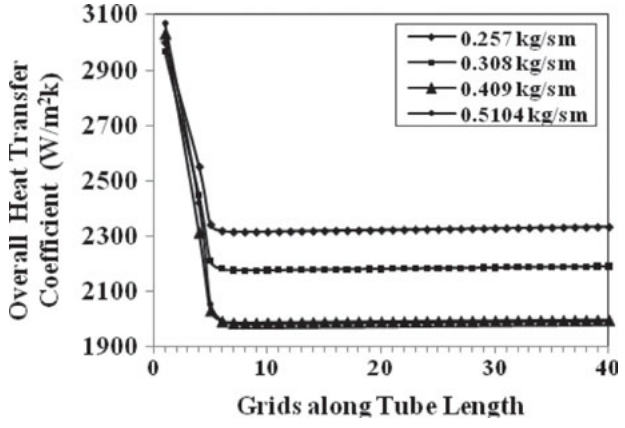

Fig. 15. Overall Heat transfer coefficient along tube length for different solution flow rates. (Solution inlet temperature 102°C, wall temperature 106.5°C, tube length 1.3 m)

flow rate, the film thickness was getting wider and provided better insulation between the heated wall and evaporating interface.

From both the figures, it is seen that at the entrance, where thermal boundary layer just started to develop, the heat transfer coefficient achieved its maximum value since the boundary layer thickness is minimum. However, after the first grid, as the inlet solution was getting heated by the heat coming from the condensing wall, there was a transitional temperature region where a steep decrease in the HTC values was observed. After the 5th grid, when a steady region was developed, the HTC values increased insignificantly till the end of the tube length.

4.2. Comparison between simulation and experiments

This section deals with the comparison between results from experiments and simulation. The area of investigation was distillate production under variable operating conditions. It has been mentioned earlier that condensation was not taken into account in the model. It dealt with evaporation exclusively. To see whether the developed model was appropriate in practice, the evaporated mass was compared with the produced distillate from the pilot plant. The agreement between the experiments and simulation was in the acceptable range considering the limitations in the experimental setup.

4.2.1. Changing compressor speed

Fig. 16 represents the comparison of distillate characteristics for increasing compressor speed. Distillate production increased with compressor speed as a result of higher heating medium flow rate and temperature. Total heat input to the system, hence, the wall temperature increased with compressor speed and it influenced the simulation results positively.

4.2.2. Changing brine concentration

Increasing brine concentration showed negative influence on distillate production for experiment and simulation. For higher concentration, boiling point was elevated but as the heat input was constant for a certain compressor speed and brine temperature, the distillate production decreased. The trend is supported by the simulation values, as shown in Fig. 17. However, the difference between the simulation and experimental values seems a bit high. For increasing concentration, experiments were interrupted by the aggressive corrosion rate. The circulation pumps were replaced because of damage and thick layers of salt were found over the components. It was also not possible to check the repeatability of the results due to the corrosion and damages. In simulation, these drawbacks were not considered.

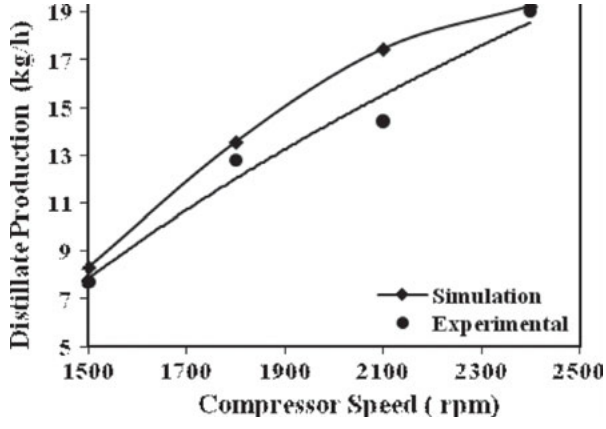

Fig. 16. Comparison of distillate characteristics with increasing compressor speed.

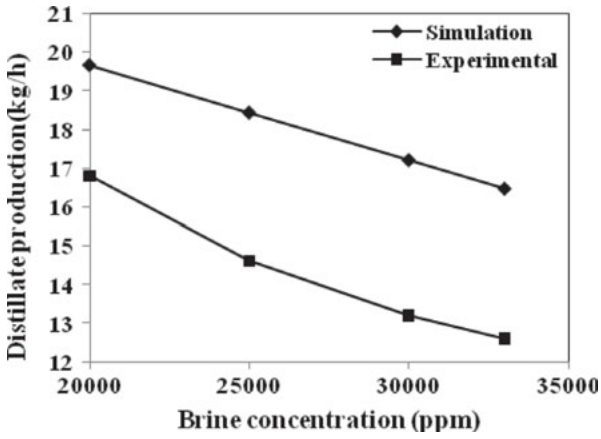

Fig. 17. Comparison of distillate production with increasing brine concentration.

4.2.3. Changing top brine temperature (TBT)

A comparison between distillate production with increasing top brine temperature for experiments and simulation is presented in Fig. 18. As there were two Effects, TBT for each Effect has been included in the figure. It is seen that for experiments, the amount of distillate produced showed the tendency to become insensitive of the brine temperature with a higher value. For values higher than 101°C (Effect 1)–99°C (Effect 2), experiments showed that the distillate production remained unchanged. However, it is seen from simulation that with increased TBT, distillate production continued to increase. For simulation the evaporated mass was compared directly with the produced distillate. No effect of the condenser wall temperature was taken into account in simulation and it was also assumed that the entire vapor generated is getting condensed to produce the distillate. But actually, the evaporated mass from one Effect condensed on the condenser (tube walls) of the other Effect. Therefore, when the solution temperature, hence, the tube wall temperature was increased, the condensation rate decreased as a result of lower cooling capability.

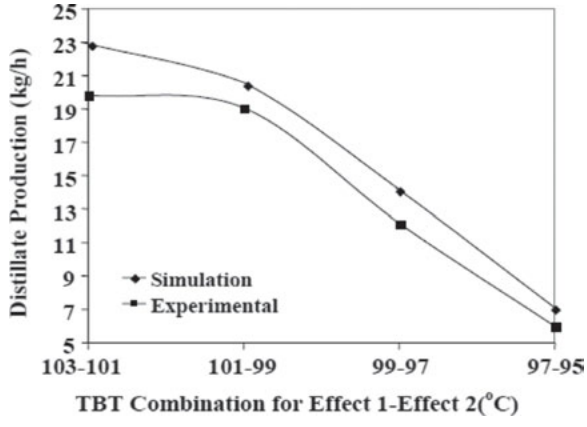

Fig. 18. Comparison of distillate production with increasing TBT.

5. Conclusions

An evaporation model was developed and validated for a vapor compression MED pilot plant. The model investigated saltwater evaporation inside a vertical falling film. Concentration and temperature changes along and across the film were explored thoroughly. Although the existing desalting process was an evaporation-condensation combination, only evaporation was looked into as experimentally the condenser side was not accessible to obtain the necessary inputs for simulation. The mass evaporated was compared with the amount of distillate from the rig. Satisfactory agreement was found between experiments and simulation except for a small region of increasing TBT. The rig produced the highest amount of distillate at a TBT of 102°C and compressor speed of 2400 rpm. With increasing feed flow rate the overall HTC as well as the evaporation rate dropped as a result of reduced residence time over the heated plate and thicker falling film. Increased concentration did not have significant effect on production compared to TBT and compressor speed. This work presents significant information on falling film evaporation depicting the nature of changing concentration and temperature inside a thin falling film. Also, results on parametric variation are included to provide a better understanding of the plant's performance under different operating conditions.

Symbols

A	—	Area of the tube surface, [m^2]
a	—	Slope for equilibrium temperature-salt concentration relation [Eq. (11)]
b	—	Constant for equilibrium temperature-salt concentration relation. [Eq. (11)]
C_{Nacl}	—	Mass fraction of Nacl
C_{water}	—	Mass fraction of water
c_p	—	Specific heat of solution, [kJ/kgK]
d	—	Tube diameter [m]
D_s	—	Diffusion coefficient , [m^2/s]
g	—	Acceleration due to gravity, [m/s^2]
U	—	Overall heat transfer coefficient [W/m^2K]
h_{fg}	—	Latent heat of evaporation [J/kg]
h_i	—	Convective heat transfer coefficient between bulk solution-interface. [W/m^2K]
h_w	—	Convective heat transfer coefficient between wall-bulk solution. [W/m^2k]
k_s	—	Thermal conductivity of solution, [W/mK]

k_w — Thermal conductivity of wall, [W/mK]
L — Tube length, [m]
$\dot{m}$ — Evaporated mass flux [kg/sm^2]
P — Pressure [bar]
T — Temperature, [°C]
T_o — Inlet Temperature, [°C]
T_{wall} — Wall Temperature, [°C]
u — Velocity along flow, [m/s]
u_{ave} — Average velocity along flow, [m/s]
v — Velocity along film thickness, [m/s]
W — Width of the equivalent plate to tube, [m]
X — Axis along the direction of solution flow
Y — Axis along film thickness

Greek letters

Γ — Solution flow rate per unit width, [kg/sm]
Γ_o — Inlet solution flow rate, [kg/sm]
δ — Film Thickness, [m]
α — Thermal diffusivity, [m^2/s]
μ — Dynamic viscocity of solution, [kg/ms]
υ — Kinematic viscocity of solution, [m^2/s]
ρ_s — Density of solution, [kg/m^3]
τ — Shear stress, [Pa]
ξ — Dimensionless form of x axis
ψ — Dimensionless form of y axis

References

[1] H. Raach and J. Mitrovic, Simulation of heat and mass transfer in a multi effect distillation plant for seawater desalination, Desalination, 204 (2007) 416–422.
[2] K. Fahem, S. Ben Jabrallah, A. Belghith and J.P. Corriou, Numerical simulation of the behaviour of a distillation cell with influence of the characteristics of the heating wall, Desalination, 201(2006) 185–197.
[3] S. Ben Jabrallah, A. Belghith and J.P. Corriou, Convective heat and mass transfer with evaporation of a falling film in a cavity, Int. J. Therm. Sci., 45(1) (2006) 16–28.
[4] M. El Haj Assad and M.J. Lampinen, Mathematical modeling of falling liquid film evaporation process, Int. J. Refrig., 25 (2002) 985–991.
[5] Y.L. Tsay and T.F. Lin, Evaporation of a heated falling liquid film into a laminar gas stream, Exp. Therm Fluid Sci., 11 (1995) 61–71.
[6] D.T. Hughes and T.R. Bott, Minimum thickness of a liquid film flowing down a vertical tube, Int. J. Heat Mass Transfer, 41 (1998) 253–260.
[7] E.N. Ganic and M.N. Roppo, A note on heat transfer to falling liquid films on vertical tubes, Letters in Heat and Mass Transfer, 7 (1980) 145–154.
[8] G. Aly, A. Al-Haddad and M. Abdel-Jawad, Parametric study on falling-film seawater desalination, Desalination, 65 (1987) 43–55.
[9] W.X. Jin, S.C. Low and T. Quek, Preliminary experimental study of falling film heat transfer on a vertical doubly fluted plate, Desalination, 152 (2003) 201–206.
[10] A.D. Al-Ansari and I. Owen, Thermal and Hydrodynamic Analysis of the condensation and evaporation processes in horizontal tube desalination plant, Int. J. Heat Mass Transfer, 42 1999 1633–1644.
[11] M.R. Islam, Performance evaluation of absorbers for vapor absorption cooling systems, Ph.D Thesis, The National University of Singapore, 2002.
[12] G. Grossman, Simultaneous heat and mass transfer in film absorption under laminar flow, Int. J. Heat Mass Transfer, 6 (1983) 357–371.
[13] R.B. Bird, W.E. Stewart and Lightfoot, E.N. Transport Phenomena, Wiley & Sons, Inc., 1960.